Journal of Materials Chemistry A

PAPER

View Article Online
View Journal | View Issue

Cite this: J. Mater. Chem. A, 2015, 3, 20749

Synthesis of boron nitride nanostructures from borates of alkali and alkaline earth metals†

Andrei T. Matveev,*[a] Konstantin L. Firestein,[a] Alexander E. Steinman,[a] Andrey M. Kovalskii,[a] Irina V. Sukhorukova,[a] Oleg I. Lebedev,[b] Dmitry V. Shtansky*[a] and Dmitri Golberg*[c]

Received 28th July 2015
Accepted 4th September 2015

DOI: 10.1039/c5ta05831g

www.rsc.org/MaterialsA

Reactions of borates of alkali and alkaline earth metals with ammonia in a temperature range of 950–1250 °C are explored with respect to the nano-boron nitride syntheses. $M_2O(MO)\cdot nB_2O_3$ borates, where M_2 = Li, Na, K, and M = Mg, Ca, Sr, Ba are studied for a molar ratio n = 0.5–5.0. It is found that various boron nitride (BN) nanostructures such as BN-nanotubes (BNNTs), graphene-like BN petals (BNGPs), and columnar porous BN (BNP) flakes grow depending on the borate composition and synthesis temperature. Both morphology and yield of BN-nanostructures depend on the basicity of the metal oxide and its fraction in the precursor borate. Borates of Li, Mg, and Ca demonstrate the highest ability to produce BNNTs. Borates of Na and K produce BNGPs in the whole range of investigated n values and temperatures. BNP flakes with pores of 10–100 nm are formed from Mg-borates with n > 3.

1 Introduction

Hexagonal boron nitride (BN) is widely used in modern technologies due to a complex of physical and chemical properties such as high thermal stability, resistance to oxidation at high temperatures, chemical resistance, dielectric strength, low specific density, and low coefficient of friction. α-BN forms a series of nanostructures: nanoparticles – smooth or with a petal-like surface, and solid or hollow;[1–5] nanotubes – cylindrical, polygonal, spiral, bamboo-like, and others;[6] thin graphene-like petals;[7] nanocages;[8] nanocones[9] and mesoporous BN.[10] BN nanostructures are actively studied as materials for nano-optical-magnetic devices, catalysis and biotechnologies.[11–14] BN nanostructures retain the physical–chemical properties inherent to the bulk BN. In addition, straight BN nanotubes (BNNTs) and graphene-like BN petals (BNGPs) exhibit exceptionally high mechanical strength (~33 GPa for BNNTs,[15] and ~130 GPa for BNGPs[16]) because of the perfection in their crystal structure. This makes BNNTs and BNGPs promising materials for producing high-strength composites based on polymer, ceramic and metal matrixes.

At present, several methods have been developed to synthesize BNNTs with a high yield, *i.e.* tens of grams per hour: plasma-chemical method in a gaseous mixture of (N_2 + H_2) at a gas pressure of 1 bar,[17] plasma-chemical method in a N_2 atmosphere at a gas pressure of 10 bar,[18] a method of annealing a porous boron-containing precursor,[19] and ball-milling and annealing method.[20–23] Both plasma-chemical methods provide thin (10–20 nm), highly crystalline BNNTs that form a web-like material. Despite the perfection of individual nanotubes, such a material is not suitable for manufacturing composites because of the entanglement of BNNTs. Annealing of the porous boron-containing precursor resulted in four types of BNNTs: wave-like, bamboo-like, bubble-chain, and cylindrical. The first three BNNT types have low tensile strength due to a large number of morphological inhomogeneities and cannot be used as a reinforcing nanophase. Cylindrical nanotubes produced by annealing appear to be strongly curved and twisted, which is apparently a consequence of a large number of structural defects, thus they exhibit tensile strength inferior to highly crystalline BNNTs. A ball-milling and annealing method provides discrete BNNTs in large quantities suitable for using as reinforcements. However, the shortcomings of the method limiting its wide commercial applications are the requirement of a long ball-milling activation stage of the boron precursor, *i.e.* 100 h, and a relatively small amount of the material that can be treated in a ball mill. Therefore, development of a scalable method for the synthesis of high quality discrete BNNTs suitable for the fabrication of strong yet light composite materials still remains a challenge.

Discrete and straight perfectly structured BNNTs are produced in a boron oxide CVD process (BOCVD) based on gas transport reactions of boron oxide vapour and ammonia.[24] Today this method allows obtaining BNNTs at a gram level in a single experimental run. In order to further increase the

[a]National University of Science and Technology "MISIS", Leninskiy prospect 4, Moscow, 119049, Russian Federation. E-mail: a.matveev@yahoo.com; shtansky@shs.misis.ru

[b]CRISMAT, UMR 6508, CNRS-ENSICAEN, 6Bd Marechal Juin, Caen, 14050, France

[c]National Institute for Materials Science (NIMS), Namiki 1, Ibaraki, Tsukuba, 3050044, Japan. E-mail: golberg.dmitri@nims.go.jp

† Electronic supplementary information (ESI) available. See DOI: 10.1039/c5ta05831g

efficiency of this method an adequate growth model of BNNTs should be ensured. The most common scheme of BOCVD assumes redox reactions between boron and a metal oxide, resulting in the formation of boron oxide vapor,[25] which then reacts with ammonia to form BN:

$$MeO_x(s) + B(s) \rightarrow B_2O_2(g) + Me(v),$$
where Me = Mg, Ga, Si, Fe, Ni, V[25–29]

$$B_2O_2(g) + 2NH_3(g) \rightarrow 2BN(s) + 2H_2O(v) + H_2(g),$$

where "s", "g", "v" indicate solid, gas or vapor state of the reagents, correspondingly. Oxides of lithium and magnesium are most often used in the BNNT syntheses as they lead to the highest nanotube yields.

For the lithium oxide precursor another scheme was proposed.[30] In this case the redox reactions proceed in the reverse direction in a lower temperature zone of the reactor and lithium reduces the boron oxide vapour forming boron and producing BNNTs while reacting with ammonia:

$$2Li(v) + BO(g) \rightarrow Li_2O(v) + B(s)$$

$$2B(s) + 2NH_3(g) \rightarrow 2BN(s) + 3H_2(g)$$

Apart from these two synthesis schemes a third "Borate Approach" scheme is also possible, *i.e.* the formation of BNNTs occurs from borates which are formed by reactions of metal oxides with boron and then either move into the colder zone of the reactor as a vapour, or are crystallized on the reactor walls during the condensation of boron oxide and metal oxide vapours. In favour of the latter scheme we may point out the rather high volatility of alkali or alkaline earth metal borates at temperatures common for the BOCVD process, as was observed in our experiments on thermo-gravimetric analysis (not discussed here).

It is known that hexagonal BN is formed *via* a reaction of sodium tetraborate with ammonia at temperatures as low as 850 °C.[31] In our previous work it has been shown that a lithium borate-based melt promotes the synthesis of BNNTs.[32] Thin-walled BN microtubes were obtained from a precursor mixture of Li_2CO_3 and B through a Li_2O–B_2O_3 eutectic reaction.[33] Also BNNTs were synthesized through a reaction of barium metaborate with ammonia at 1300 °C.[34] These facts encouraged us to investigate the reactions of borates with ammonia. Thus in this study we thoroughly studied the syntheses of BN nanostructures *via* the direct reactions of alkali and alkaline earth metal borates with ammonia.

2 Experimental

2.1 Materials

$M_2O \cdot nB_2O_3$ borates, where M = Li, Na, K with a molar content of boron oxide in the range of n = 0.5–3.0, and $MO \cdot nB_2O_3$ borates, where M = Mg, Ca, Sr, Ba with a molar content of boron oxide in the range of n = 0.5–5.0, were used as precursors. Carbonates of alkali metals and hydroxides of alkaline earth metals were used for the synthesis of corresponding borates through their reaction with boric acid. All reagents were of chemical grade. Weighted mixtures of reagents were ground in an alumina mortar with addition of distilled water. All mixtures (except with lithium carbonate) were calcined at 800 °C for 1 h, while mixtures with Li_2CO_3 were calcined at 600 °C for 1 h. Then the mixtures were thoroughly ground in isopropanol and subjected to reaction with ammonia. Ammonia of 99.98% purity was used for the syntheses.

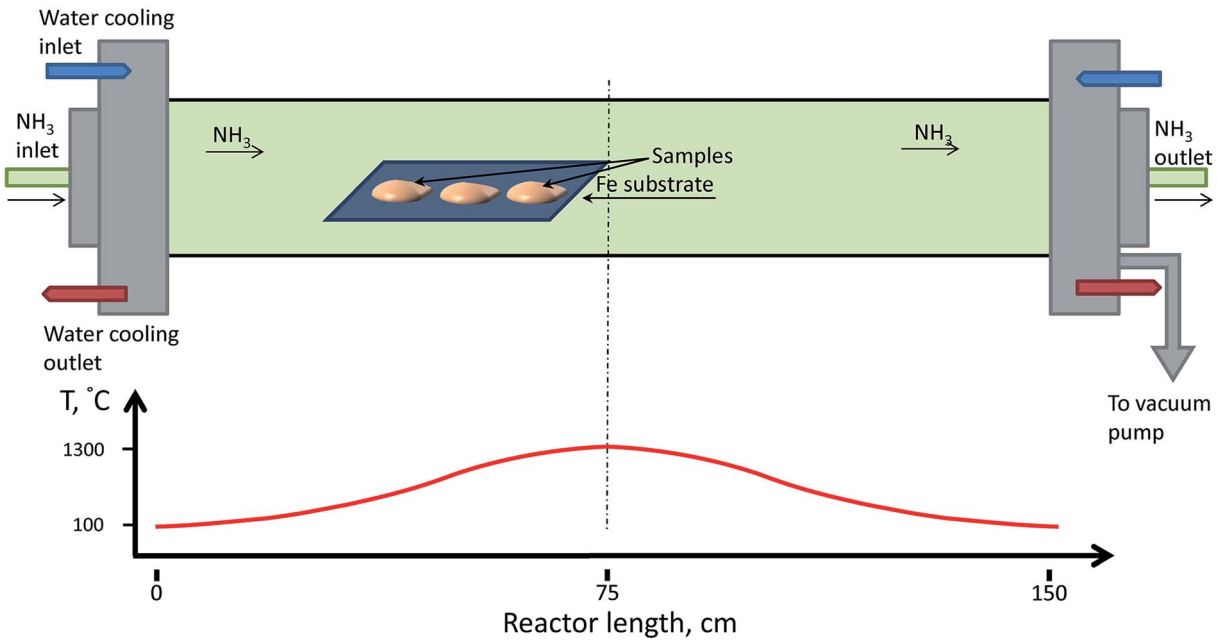

Fig. 1 Schematic view of the experimental set-up with the temperature profile within the reactor measured for the pre-set temperature of 1300 °C.

2.2 Experimental set-up

Reactions of borates of alkali and alkaline earth metals with ammonia were performed in a horizontal tubular reactor consisting of an alumina tube with tight flanges. Powdered precursor borates suspended in isopropanol were dropped on the surface of a low carbon steel plate and placed in a temperature gradient zone of the reactor. Iron was selected as a substrate material due to its chemical stability in ammonia at high temperatures and its inertness to borate melts. The reactor temperature profile at 1300 °C was measured in advance. After attaining a base vacuum pressure of 10^{-2} mbar, the reactor was filled with ammonia at a flow rate of 100 cm^3 min^{-1}. Then the reactor was heated to the desired temperature with a ramp of 275 °C h^{-1}, held for 1 h, and then cooled down naturally. A schematic set-up is shown in Fig. 1.

2.3 Characterization

The morphology of the synthesized products was studied using a scanning electron microscope JEOL JSM-7600F. Transmission electron microscopy (TEM) including high resolution TEM (HRTEM) and selected-area electron diffraction (SAED) were carried out using a Tecnai G2 30 UT microscope operated at 300 kV. HRTEM was performed on a JEM ARM-200F cold field emission gun (FEG) probe and lens aberration corrected microscope operated at 200 kV and equipped with a wide angle CENTURIO EDX detector and Quantum Gatan imaging filter (GIF). The chemical compositions were analyzed by energy-dispersive X-ray (EDX) spectroscopy using an 80 mm^2 X-Max EDX detector (Oxford Instruments). The phase composition was determined by X-ray diffraction using an X-ray diffractometer DRON-3 operated under Cu Kα radiation. The structural perfectness of BN nanostructure arrays was confirmed using confocal Raman spectroscopy using a NT-MDT NTEGRA Spectra instrument with an excitation wavelength of 473 nm. The volume fraction of synthesized BN nanophases was roughly estimated using SEM observations.

3 Results and discussion

In total 144 nano-BN samples have been synthesized under various conditions and thoroughly analyzed. The synthesis temperatures and compositions of the studied borates are represented in Tables S1 and S2 (see the ESI†). Lithium and magnesium borates were studied in more detail because Li_2O and MgO provide the highest (among other oxides) yields of the BNNTs under the BOCVD method.

X-ray analysis of the synthesized samples revealed that the hexagonal BN with crystal lattice parameters of $a = 2.50$ Å and $c = 6.69$ Å was the major phase after the reaction of borates of alkali and alkaline earth metals with ammonia in the temperature range of 950–1250 °C. The X-ray diffraction pattern of the reaction products of lithium tetraborate with ammonia at 1200 °C is presented as an example in Fig. S1 (ESI†). At synthesis temperatures below 1000 °C, a small amount of the precursor borates was observed. It should be noted that in some cases discussed below, a certain amount of borates was also observed in the samples synthesized at 1150 °C and even at 1250 °C.

SEM analysis revealed that the samples synthesized from borates contained BN nanostructures of different morphologies: BNNTs, nano- and microfibers (BNFs), BNGPs, and BNPs. As shown below, the presence of these nanostructures depended on both the precursor borate composition and synthesis temperature. Apart from these structures, some amount of BN particles of other morphologies (plate-like, or elongated globular, or diverse shapes) was observed in all samples.

The SEM image of typical nanotubes synthesized *via* the reaction of borates of alkali or alkaline earth metals and ammonia is shown in Fig. 2a. It should be noted that for all investigated borate compositions and synthesis temperatures such nanotubes were the sole phase observed. The average diameter and length of the nanotubes were 50–100 nm and tens of micrometers, respectively (the inset in Fig. 2a). Note that the thinner nanotubes of about 30 nm in external diameter and thicker ones up to 200 nm were also seen.

The HRTEM image and the corresponding SAED pattern of a single multiwalled BNNT are presented in Fig. 2b and c. The BNNT walls consist of 7 BN layers with a uniform inter-layer spacing of 0.33 nm which is a fingerprint of the (002) planes of h-BN. Clear lattice fringes in the HRTEM image and sharp electron diffraction spots confirm the tube structural perfectness. The high quality of the BNNTs was almost independent of the synthesis temperatures and precursor borate compositions. The high quality of the BNNT array was confirmed by Raman spectroscopy. A typical Raman spectrum taken from BNNTs is shown in Fig. 2d. The sharp peak at 1365 cm^{-1} was assigned to the E_{2g} mode of the h-BN. The FWHM of this band is only 18 cm^{-1} indicating excellent crystallinity.

The typical SEM image of BNFs is presented in Fig. 3a. The diameter of fibers increased with increasing synthesis temperature and reached several micrometers at 1250 °C, whereas their length reduced. At low temperatures (1100 °C and below) BNFs can be as thin as BNNTs and may have an average diameter of about 100 nm or even less (thin BNFs are seen in Fig. 3a). Note that BNFs may also have an inner channel, similar to BNNTs.[32] Note, however, that the BNNTs appear mostly straight (or smoothly curved) with a constant diameter along the entire length (Fig. 2a), whereas BNFs are strongly curled and show a variable diameter along their lengths (Fig. 3a).

These morphological features of BNNTs and BNFs are related to different defects in their crystal structures: BNNTs are highly ordered, being in fact single-crystal objects, whereas BNFs are polycrystalline materials. Thus, as the main factor in the classification of BNNTs and BNFs we consider their crystalline perfection, which manifests itself in their morphological features. This approach allows classifying and even estimating the volume fraction of the nanotubes and their nanosized BNF counterparts under detailed SEM observations.

BNGPs were observed to appear on the surface of BNNTs, BNFs, borates, or BN particles. The SEM image of the BNGPs synthesized from sodium tetraborate at 1000 °C is shown in Fig. 4a.

The Raman spectrum for this sample is displayed in the inset in Fig. 4a. The E_{2g} mode peak of the h-BN at 1365 cm^{-1} has an

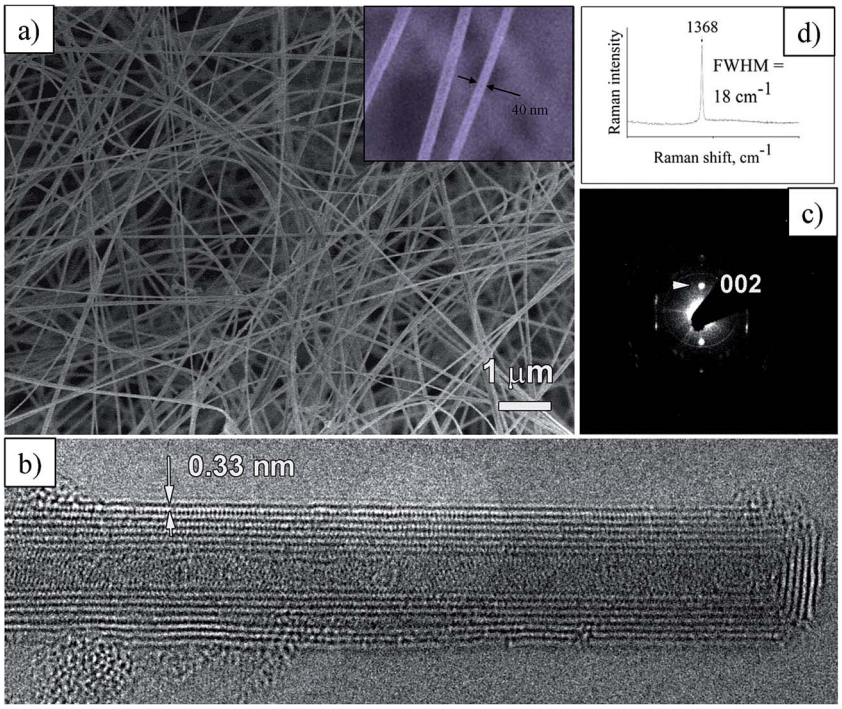

Fig. 2 (a) SEM image of typical BNNTs synthesized *via* the reaction of $Li_2O{\cdot}2B_2O_3$ with ammonia at 1000 °C. The high magnification SEM image of the BNNTs is given in the inset. (b) Bright field HRTEM image of an individual multi-walled BN nanotube; and (c) corresponding SAED pattern. (d) A Raman spectrum from the BNNT array shown in panel (a).

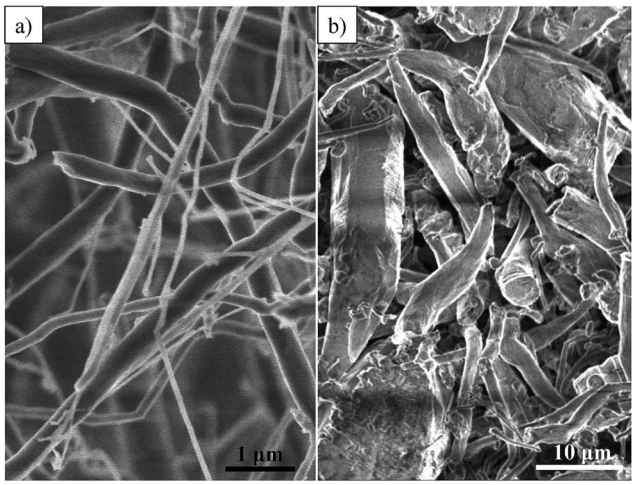

Fig. 3 (a) SEM image of typical BNFs obtained after the reaction of $Li_2O{\cdot}2B_2O_3$ with ammonia at 1100 °C. BNFs thinner than 100 nm are seen. (b) SEM image of large BN particles.

FWHM of about 24 cm^{-1}. This value is larger than that for the BNNTs synthesized at 1100 °C from the Li-borate (Fig. 2d). This indicates that the material has a relatively lower crystal ordering, which may be attributed to the lower synthesis temperature. The low magnification TEM image (Fig. 4b) illustrates BNGP and a thin multi-walled BNNT. The HRTEM image and the corresponding FFT pattern demonstrate that the single BN-petal appears as a thin folded hexagonal BN-layer consisting of only a few atomically thin BN-sheets (Fig. 4c).

BNNTs, BNFs, and BNGPs were observed together with BN particles, which may appear as plate-like, globular, or free-shape morphologies. The size of the BN particles varies from submicrometers to several tens of micrometers depending on the synthesis temperature. The SEM image of elongated globular BN particles is presented in Fig. 3b.

The summarized results on the synthesis of BN nanostructures by the direct reaction of alkali and alkaline earth metal borates with ammonia are shown in Fig. 5 and 6. Red dots mark the tested compositions and synthesis temperatures, as described in Tables S1 and S2.† Red numbers, n, indicate the number of B_2O_3 moles in the precursor borates. The coloured regions represent the areas where the growth of the aforementioned BN structures (BNNTs, BNFs, and BNGPs) was documented and the intensity of the colours qualitatively reflects the product yields of a given BN nanostructure. Each coloured region indicates the synthesis conditions under which only one particular type of BN nanostructure was observed. This means that a fraction of such a specific BN nanophase is 100%. This is the case for BNFs from Li-borates for $n < 1$ at all investigated temperatures, for BNNTs from Ca-borates for $n = 0.5$ and at 1100 °C, and for BNGPs: from Na-borates, for $n = 3$, and for other n values below 1100 °C, for K-borates below 1200 °C, and for Sr- and Ba-borates at any investigated temperatures and n values. In multi-coloured regions more than one BN nanophase was detected. For example, while using Li-borates, BNGPs (green area) coexist with BNNTs (red area) and with BNFs (blue area). This means that BNGPs were grown either on BNNTs, or on BNFs (Fig. S2†). In this case the accurate estimation of the

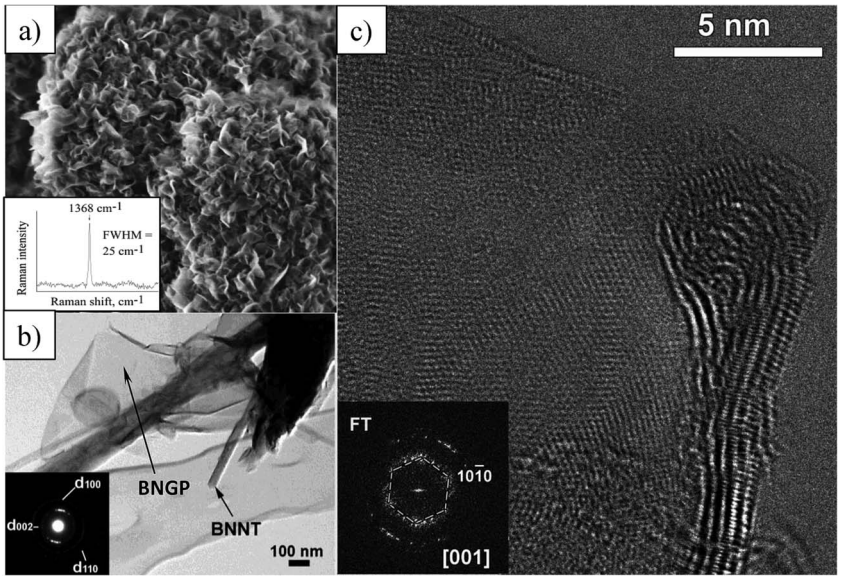

Fig. 4 (a) SEM image of typical BNGPs grown from sodium tetraborate at 1000 °C. The inset shows the Raman spectrum recorded for this sample. (b) Low magnification bright field TEM image of BNNT and BNGP. The inset shows the corresponding SAED pattern. (c) HRTEM image of an individual BNGP with peculiar bending. The inset depicts the corresponding fast Fourier transform (FFT) pattern from the flat part close to the [001] zone axis.

volume fraction of BNNTs and BNGPs is complicated because of very different specific volumes of different morphologies. Therefore, we roughly evaluate it to be 50 : 50 from comparison of the thicknesses of BNNTs and the BNGP layers covering them. For syntheses which are not included in the coloured regions, BN nanophases were not observed and only big bulky BN particles were detected.

Borates of Li, Na, and K reacted with ammonia in different ways (Fig. 5a). Although lithium borates reacted with ammonia to form all the three above-mentioned BN morphological types, BNNTs and BNFs were the predominant ones. Nanotubes and nanofibers were observed in a wider range of compositions and synthesis temperatures than the other BN morphologies. In contrast, the sodium and potassium borates tended to form the BNGPs, whereas the growth of BNNTs and/or BNFs was observed in a narrower range of compositions and synthesis temperatures. Since the sodium and potassium borates demonstrated a very similar reaction with ammonia the latter system was not studied in detail. Overall, the obtained results suggest that BN nanostructure morphologies formed upon the reactions of borates with ammonia depend on the (i) synthesis temperature, (ii) nature of the metal oxide (Li_2O, Na_2O, or K_2O), and (iii) its content. X-ray analysis of the Li-borate reaction products with ammonia revealed that the samples synthesized at 1100 °C from borate with $n = 3$ consisted of only h-BN, whereas the samples synthesized from borate with $n = 0.5$ contained a notable amount of the unreacted precursor borate which was observed even at 1150 °C. This indicates that borates with a higher Li_2O content exhibit slower reaction kinetics with ammonia.

The data on the reactions of Ca, Sr and Ba borates with ammonia are shown in Fig. 5b. These borates reacted with ammonia to form three types of nanostructures: BNNTs, BNFs, and BNGPs. The dimension of the *n*-T region, where the growth of BNNTs was well documented, and the yield of BNNTs depend on the type of alkaline earth metal oxide. Both values gradually decrease in the order $CaO \cdot nB_2O_3$, $SrO \cdot nB_2O_3$, $BaO \cdot nB_2O_3$, similar to the alkali metal borates. And Mg-borates start this sequence. The formation of BNNTs was observed in a wide *n*-T region at a high yield (Fig. 6a). It was shown that borates containing more basic oxides are more stable with regard to their decomposition into B_2O_3 and the corresponding metaborate formation.[35] The stability of borates increases in the sequences $Li_2O \cdot nB_2O_3$, $Na_2O \cdot nB_2O_3$, $K_2O \cdot nB_2O_3$ and $MgO \cdot nB_2O_3$, $CaO \cdot nB_2O_3$, $SrO \cdot nB_2O_3$, $BaO \cdot nB_2O_3$ for alkali metal and alkaline earth metal borates, respectively. This suggests that the growth of BNNTs during reactions of borates with ammonia is related to the degree of borate dissociation, *i.e.* the less stable borate produces the higher amount of BNNTs.

Two scenarios are commonly accounted for the growth of nanotubes, *i.e.* from the tip or from the base of a nanotube. The former scenario is associated with a vapor–liquid–solid (VLS) process assuming the presence of catalyst particles at the tips of growing nanotubes. Since we did not observe any particles at the tips of BNNTs, we suppose that their growth during the reactions of borates with ammonia was realized *via* a base mode, *i.e.* from a liquid *via* a liquid–solid process. In such a process the composition of the feeding liquid is crucial. Assuming that the relative content of metaborates and B_2O_3 in borate melts under the reaction in ammonia also continuously increases with decrease in basicity of the metal oxides, we can conclude that the growth of the BNNTs occurs from one of these liquids. Signs of the presence of a liquid at high temperatures are clearly seen in the SEM image of a sample with $n = 1.5$

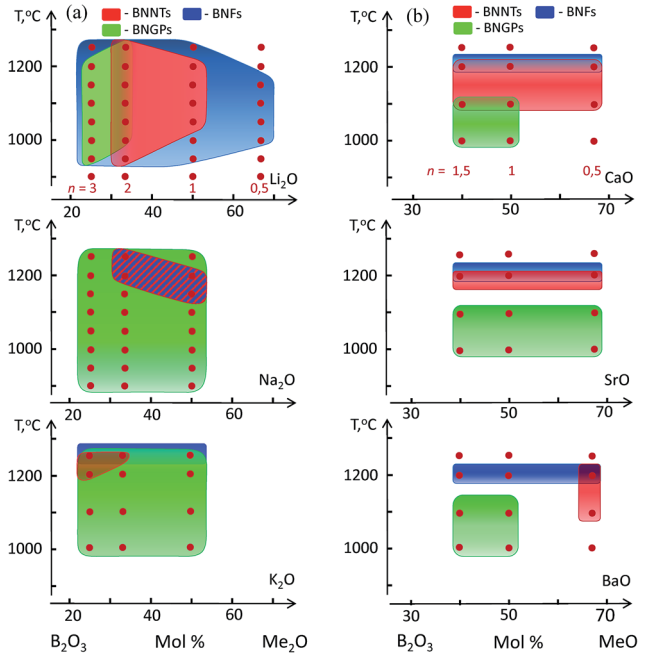

Fig. 5 Diagrams of BN-product yields obtained in reactions of borates of (a) alkali and (b) alkaline-earth metals with ammonia at different temperatures. Red dots mark the samples synthesized. The synthesis condition area for each type of nanostructure is shown in various colours. The appearance of each coloured region corresponds to a given type of BN nanostructure: BNNTs, BNFs, and BNGPs. The synthesis of BN particles is not shown because they exist in all samples in some amounts. Number n on the upper row panels indicates the number of B_2O_3 moles in the borate precursors.

reacted with ammonia at 1200 °C (Fig. S3†). Besides the BNNTs this sample contains a reaction product having a smooth surface and glassy-like appearance indicating its origin from a liquid. The composition of the solidified liquid could not be, however, determined by EDX analysis due to its marginal presence.

To test the hypothesis that the composition of the feeding liquid is responsible for the BNNTs growth, a series of syntheses in argon instead of ammonia was performed. Fig. 6b represents the data on the Mg borate samples heated in argon (until the pre-set temperature), reacted with ammonia for 1 h, and cooled down in ammonia. Fig. 6b also illustrates a part of the MgO–B_2O_3 phase diagram.[36] This diagram shows that above 988 °C $MgO \cdot B_2O_3$ melts incongruently and above 1142 °C two immiscible liquids with low (liquid A) and high (liquid B) MgO contents appear. SEM analysis of the synthesized products revealed that the samples synthesized at or above 1200 °C also consisted of two phases: BNNTs and faceted or round particles (Fig. 7). The particles have a clean surface manifesting their inertness to ammonia at high temperatures. EDX analysis of these particles gave a relative ratio of B to Mg close to 2 (Fig. 7), indicating their formation from the liquid B with the MgO content close to that in magnesium metaborate. Therefore, it is reasonably assumed that BNNTs have been grown from the secondary liquid A with a low MgO content. The higher yield of BNNTs and their greater length in samples with a higher B_2O_3 content (and thus having more liquid A at high temperatures) further support this conclusion. SEM images of the samples with $n = 3.5$ and $n = 1.5$ heated in argon and reacted with ammonia at 1200 °C are represented in Fig. S4.†

To summarize, the reactions of magnesium and lithium borates with ammonia have several common features in terms of the growth of BNNTs. First of all, they demonstrated the highest ability among other borates to produce BNNTs *via* a direct reaction with ammonia. Secondly, the yield of BNNTs increased with increasing content of boron oxide above the metaborate composition (that is for $n > 1$). Thirdly, lithium and magnesium borates with a high content of the metal oxides ($n = 0.5$ for Li-borates, and $n = 1$ for Mg-borates) demonstrated almost complete inertness to ammonia at all studied temperatures. The similar behavior of both systems allowed us to suggest that the growth of BNNTs in the Li-borate system also occurs from a liquid with a low content of lithium oxide.

Chemical reactions between ammonia and magnesium borates with $n = 0.5$–2.5 at relatively low temperatures of 1000–1100 °C resulted in the formation of BNGPs. Their size and amount in the samples with $n = 0.5$ were small, but quickly increased with increasing n (not shown here), suggesting that the growth of BNGPs was associated with the boron oxide based liquid, the amount of which increased with n. Thus, the growth of BNNTs and BNGPs appeared to occur from the same boron oxide based liquid having a low MgO content. At lower temperatures, BNGPs grew predominantly, whereas at higher

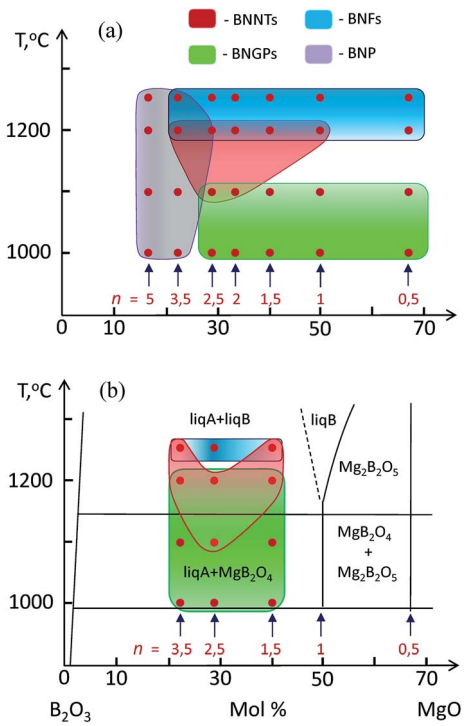

Fig. 6 Diagrams of BN-products obtained after reactions of Mg borates with ammonia at different temperatures: (a) heating in ammonia, isothermal holding in ammonia for 1 h, and cooling in ammonia; (b) heating in argon, isothermal holding in ammonia for 1 h, and cooling in ammonia.

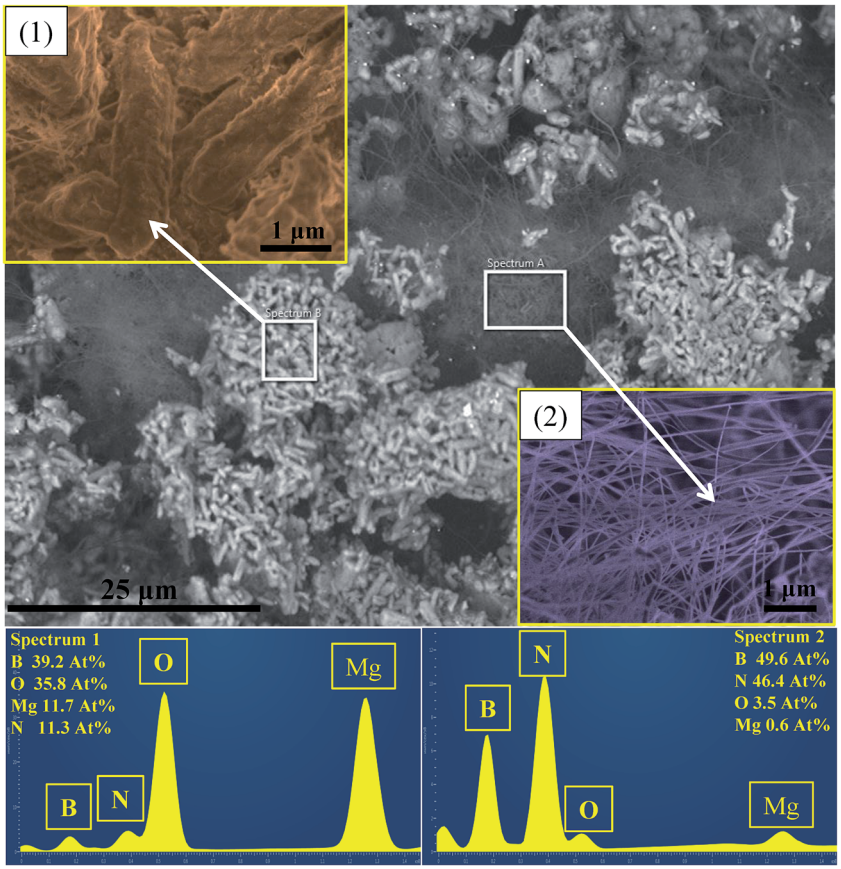

Fig. 7 (a) SEM image of a sample synthesized at 1250 °C from $MgO \cdot 3.5B_2O_3$ heated in argon. Insets (1) and (2) show SEM images at higher magnifications taken from the framed areas. The EDX spectra revealing the elemental compositions at different surface locations are also shown.

temperatures BNNT growth took place. A similar tendency was observed in the case of the alkali and alkaline earth oxide borates (Fig. 5). At 1200 °C, BNFs were seen along with BNNTs and their amount and thickness drastically increased with temperature. So, at 1250 °C only thick BNFs and large BN particles were observed. The growth model of BNNTs and BNFs (due to reactions of the borates with ammonia) is similar to that previously reported for the BOCVD growth of BNNTs[32] and can be described as follows: BNNTs and BNFs nucleated and grew from a boron oxide based liquid comprising some amount of dissolved alkali or alkaline earth metal oxides. The models differ in the source of boron oxide feeding the growth of BNNTs: boron oxide vapour[32] or a boron oxide based liquid. The effectiveness of various borates in producing BNNTs may be related to a borate liquid network structure, depending on the metal oxide and its concentration.[37]

Interestingly, the magnesium borates produced four types of BN nanostructures. Besides three already discussed types, *e.g.* BNNTs, BNFs, and BNGPs, a porous BN (BNP) structure was formed (Fig. 6a). In all the samples synthesized from Mg-borates with $n \geq 2.5$ BNP was observed in the temperature range of 1000–1250 °C. The volume fraction of BNP increased with n and it became the only phase in the samples with $n = 5$. This indicates that the BNP material was also formed from a boron oxide based liquid. SEM images of the BNP synthesized from $MgO \cdot 5B_2O_3$ at 1000 °C are presented in Fig. 8. The BNP contains pores with the diameter in the range of 10–100 nm. The SEM image of the BNP fracture surface reveals a columnar structure composed of grains 0.5–1.0 μm in length and 200–300 nm in width. The size of both grains and pores did not depend on the temperature. This indicates that the BNP growth was completed at relatively low temperatures (below 1000 °C) from the liquid A.

We can assume that the columnar structure developed due to water vapour coming out from the sample as a result of the reaction

$$B_2O_3(l) + 2NH_3(g) \rightarrow 2BN(s) + 3H_2O(v)$$

Finally, we envisage that the obtained results demonstrate that the reactions of alkali and alkaline earth metal borates with ammonia can serve as a solid basis for the development of a new "Borate Approach" toward the scalable syntheses of versatile BN nanostructures. By appropriate selection of the synthesis parameters (composition of the borate precursor and temperature), various BN nanostructures can be selectively synthesized. The present work was mostly dedicated to different fundamental aspects of the physical–chemical interactions of borates with ammonia. Because of this both borate precursors and synthesized BN nanophases had only weights of tens of

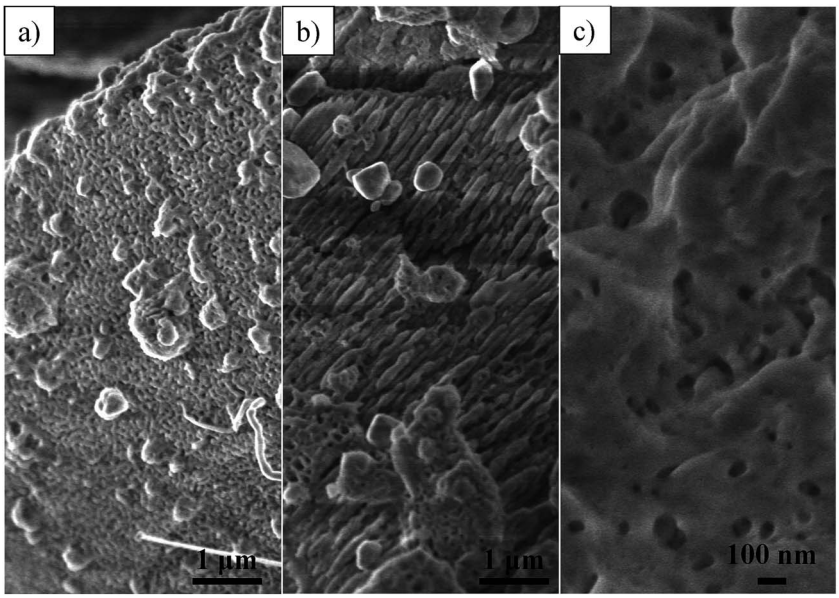

Fig. 8 SEM micrographs of BNP synthesized *via* the reaction of $MgO \cdot 5B_2O_3$ with ammonia: (a and c) top view, (b) cross-sectional view.

milligrams, however the described method can be easily scaled up using continuous reactors of conveyor- or spindle-like types to produce BNGPs and BNNTs at a rate of grams or tens of grams per hour, correspondingly. To the best of our knowledge such yields would be the highest ever announced rates for graphene-like BNGP production. It is noted that discrete BNNTs with comparable yields can also be produced by the "ball-milling and annealing" method,[20–23] however, the method proposed by us has several important advantages: (i) one stage processing (no need for long ball-milling processing times), (ii) faster synthesis (1 h instead of 3–6 h), and (iii) use of cheaper boron-containing precursors (borates instead of amorphous boron).

4 Conclusions

Various BN nanostructures such as nanotubes, graphene-like petals, and porous materials were obtained with high yields *via* a direct reaction of ammonia with alkali and alkaline earth metal borates, $M_2O(MO) \cdot nB_2O_3$ (M_2 = Li, Na, K and M = Mg, Ca, Sr, Ba), within 1 h at moderate temperatures of 950–1250 °C. Both the BN nanostructure type and its yield depended on the basicity of the metal oxide, its concentration, and the synthesis temperature. The highest yield of BN nanotubes was documented while using Li-borates with mole fractions of B_2O_3 n = 1.0–2.0, Mg-borates with n = 2.0–3.5, and Ca-borates with n = 1.0–1.5. The highest yield of graphene-like petals was observed when Na- and K-borates were utilized. The highest yield of porous BN was demonstrated from Mg-borate with n = 5.0. The yield of BN nanotubes increased when the molar ratio of alkali or alkaline earth metal oxide to boron oxide was decreased below 1. The proposed model assumes that the BN nanostructures were grown from a boron oxide based liquid with a relatively low amount of dissolved alkali or alkaline earth metal oxides. In contrast, a boron oxide based liquid with a high content of alkali or alkaline earth metal oxides, close to n = 1, was shown to exhibit low activity in reactions with ammonia.

Acknowledgements

The work was supported by the Ministry of Education and Science of the Russian Federation (Increase Competitiveness Program of NUST "MISiS" No. K2-2015-001 in the frame of "Mega-Grant" award No. 11.G34.31.0061 and State task 11.1077.2014/K).

Notes and references

1 G. L. Wood, J. F. Janik, E. A. Pruss, D. Dreissig, W. J. Kroenke, T. Habereder, H. Nöth and R. T. Paine, *Chem. Mater.*, 2006, **18**, 1434.
2 C. C. Tang, Y. Bando, Y. Huang, C. Y. Zhi and D. Golberg, *Adv. Funct. Mater.*, 2008, **18**, 3653.
3 C. Xiong and W. Tu, *Eur. J. Inorg. Chem.*, 2014, **19**, 3010.
4 S. Bernard, V. Salle, J. Li, A. Brioude, M. Bechelany, U. B. Demirci and P. Miele, *J. Mater. Chem.*, 2011, **21**, 8694.
5 F. Liu, J. Yu, X. Ji and M. Qian, *ACS Appl. Mater. Interfaces*, 2015, **7**, 1824.
6 S. Kalay, Z. Yilmaz, O. Sen, M. Emanet, E. Kazanc and M. Çulha, *Beilstein J. Nanotechnol.*, 2015, **6**, 84.
7 S.-K. Kim, H. Cho, M. J. Kim, H.-J. Lee, J. Park, Y.-B. Lee, H. C. Kim, C. W. Yoon, S. W. Nam and S. O. Kang, *J. Mater. Chem. A*, 2013, **1**, 1976.
8 T. Oku, T. Kusunose, K. Niihara and K. Suganuma, *J. Mater. Chem.*, 2000, **10**, 255.
9 L. Bourgeois, Y. Bando, S. Shinozaki, K. Kurashima and T. Sato, *Acta Crystallogr., Sect. A: Found. Crystallogr.*, 1999, **55**, 168.

10 B. Rushton and R. Mokaya, *J. Mater. Chem.*, 2008, **18**, 235.
11 H. Zhao, J. Song, X. Song, Z. Yan and H. Zeng, *J. Mater. Chem. A*, 2015, **3**, 6679.
12 T. Oku, T. Kusunose, K. Niihara and K. Suganuma, *J. Mater. Chem.*, 2000, **10**, 255.
13 G. Gao, A. Mathkar, E. P. Martins, D. S. Galvão, D. Gao, P. A. da Silva Autreto, C. Sun, L. Cai and P. M. Ajayan, *J. Mater. Chem. A*, 2014, **2**, 3148.
14 I. V. Sukhorukova, I. V. Zhitnyak, A. M. Kovalskii, A. T. Matveev, O. I. Lebedev, N. A. Gloushankova, X. Li, D. Golberg and D. V. Shtansky, *ACS Appl. Mater. Interfaces*, 2015, **7**, 17217.
15 X. Wei, M. S. Wang, Y. Bando and D. Golberg, *Adv. Mater.*, 2010, **22**, 4895.
16 C. Lee, X. Wei, J. W. Kysar and J. Hone, *Science*, 2008, **321**, 385.
17 K. S. Kim, C. T. Kingston, A. Hrdina, M. B. Jakubinek, J. Guan, M. Plunkett and B. Simard, *ACS Nano*, 2014, **8**, 6211.
18 A. Fathalizadeh, T. Pham, W. Mickelson and A. Zettl, *Nano Lett.*, 2014, **14**, 4881.
19 L. Zhang, J. Wang, Y. Gu, G. Zhao, Q. Qian, J. Li, X. Pan and Z. Zhang, *Mater. Lett.*, 2012, **67**, 17.
20 L. H. Li, Y. Chen and A. M. Glushenkov, *J. Mater. Chem.*, 2010, **20**, 9679.
21 L. H. Li, Y. Chen and A. M. Glushenkov, *Nanotechnology*, 2010, **21**, 105601.
22 L. Li, L. H. Li, S. Ramakrishnan, X. J. Dai, K. Nicholas, Y. Chen, Z. Chen and X. Liu, *J. Phys. Chem. C*, 2012, **116**, 18334.
23 L. Li, L. H. Li, Y. Chen, X. J. Dai, P. R. Lamb, B. M. Cheng, M. Y. Lin and X. Liu, *Angew. Chem., Int. Ed.*, 2013, **125**, 4306.
24 C. Zhi, Y. Bando, C. Tan and D. Golberg, *Solid State Commun.*, 2005, **135**, 67.
25 C. Tang, Y. Bando, T. Sato and K. Kurashima, *Chem. Commun.*, 2002, **2**, 1290.
26 C. Tang, Y. Bando and D. Golberg, *J. Solid State Chem.*, 2004, **177**, 2670.
27 J. Li, H. Lin, Y. Chen, Q. Su and Q. Huang, *Chem. Eng. J.*, 2011, **174**, 687.
28 C. Tang, Y. Bando, Y. Huang, C. Y. Zhi and D. Golberg, *Adv. Funct. Mater.*, 2008, **18**, 3653.
29 J. S. M. Nithya and A. Pandurangan, *RSC Adv.*, 2014, **4**, 26697.
30 Y. Huang, J. Lin, C. C. Tang, Y. Bando, C. Y. Zhi, T. Zhai, B. Dierre, T. Sekiguchi and D. Golberg, *Nanotechnology*, 2011, **22**, 145602.
31 K. Ogasawara and S. Koitabashi, *EU Pat. 170 817*, 1987.
32 A. T. Matveev, K. L. Firestein, A. E. Steinman, A. M. Kovalskii, O. I. Lebedev, D. V. Shtansky and D. Golberg, *Nano Res.*, 2015, **8**, 2063.
33 Y. Huang, Y. Bando, C. Tang, C. Y. Zhi, T. Terao, B. Dierre, T. Sekiguchi and D. Golberg, *Nanotechnology*, 2009, **20**, 085705.
34 S. D. Yuan, X. X. Ding, Z. X. Huang, X. T. Huang, Z. W. Gan, C. Tang and S. R. Qi, *J. Cryst. Growth*, 2003, **256**, 67.
35 N. Vedishcheva, B. Shakhmatkin and M. Shultz, *J. Therm. Anal. Calorim.*, 1990, **36**, 2055.
36 H. M. Davis and M. A. Knight, *J. Am. Ceram. Soc.*, 1945, **28**, 97.
37 W. L. Konijnendijk and J. M. Stevels, *J. Non-Cryst. Solids*, 1975, **18**, 307.